Sea-ice control on deglacial lower cell circulation changes recorded by Drake Passage deep-sea corals

David J. Wilson [a,b]*, Torben Struve [b,c], Tina van de Flierdt [b], Tianyu Chen [d,e], Tao Li [d,e], Andrea Burke [f], Laura F. Robinson [d]

a- Institute of Earth and Planetary Sciences, University College London and Birkbeck, University of London, Gower Street, London, WC1E 6BT, UK.

b- Department of Earth Science and Engineering, Imperial College London, London, SW7 2AZ, UK

c- Marine Isotope Geochemistry, Institute for Chemistry and Biology of the Marine Environment (ICBM), University of Oldenburg, Carl-von-Ossietzky-Str. 9-11, 26129 Oldenburg, Germany

d- School of Earth Sciences, University of Bristol, Wills Memorial Building, Queens Road, Bristol, BS8 1RJ, UK

e- School of Earth Sciences and Engineering, Nanjing University, Nanjing, 210023, China

f- School of Earth and Environmental Sciences, University of St Andrews, St Andrews, KY16 9AL, UK

* Corresponding Author. Tel.: +44 20 3108 6349. Email: david.j.wilson@ucl.ac.uk

Contents:
abstract (292 words)
highlights (5)
key words (6)
main text (6594 words)
references (71)
figures (5)
supplementary tables (1)

Highlights

- First direct constraints on past water mass mixing in Lower Circumpolar Deep Water
- Reduced North Atlantic Deep Water signal in deep Southern Ocean during peak glacial
- Control by Southern Ocean stratification rather than Atlantic overturning strength
- Early deglacial Southern Ocean circulation changes linked to sea-ice retreat
- Spatially asynchronous return of North Atlantic Deep Water to deep South Atlantic

Key words

ocean circulation; deglaciation; Drake Passage; Nd isotopes; deep-sea corals; sea-ice

Abstract

The sequence of deep ocean circulation changes between the Last Glacial Maximum and the Holocene provides important insights for understanding deglacial climate change and the role of the deep ocean in the global carbon cycle. Although it is known that significant amounts of carbon were sequestered in a deep overturning cell during glacial periods and released during deglaciation, the driving mechanisms for these changes remain unresolved. Southern Ocean sea-ice has recently been proposed to play a critical role in setting the global deep ocean stratification and circulation, and hence carbon storage, but testing such conceptual and modelling studies requires data constraining past circulation changes. To this end, we present the first deglacial dataset of neodymium (Nd) isotopes measured on absolute-dated deep-sea corals from modern Lower Circumpolar Deep Water depths in the Drake Passage. Our record demonstrates deglacial variability of 2.5 ε_{Nd} units, with radiogenic values of up to ε_{Nd} = -5.9 during the Last Glacial Maximum providing evidence for a stratified glacial circulation mode with restricted incorporation of Nd from North Atlantic Deep Water in the lower cell. During the deglaciation, a renewed Atlantic influence in the deep Southern Ocean is recorded early in Heinrich Stadial 1, coincident with Antarctic sea-ice retreat, and is followed by a brief return to more Pacific-like values during the Antarctic Cold Reversal. These changes demonstrate a strong influence of Southern Ocean processes in setting deep ocean circulation and support the proposed sea-ice control on deep ocean structure. Furthermore, by constraining the Nd isotopic composition of Lower Circumpolar Deep Water in the Southern Ocean, our new data is important for interpreting deglacial circulation changes in other ocean basins and supports a spatially asynchronous return of North Atlantic Deep Water to the deep southeast and southwest Atlantic Ocean.

1. Introduction

Southern Ocean circulation dynamics play a key role in the global carbon cycle and climate system. Specifically, the combination of Southern Ocean upwelling (driven by the westerly winds) and regional buoyancy forcing sets the interior ocean structure through intermediate and deep water formation (Talley, 2013), while the Antarctic Circumpolar Current (ACC) distributes heat, salt, and carbon between the major ocean basins (Rintoul et al., 2001). As such, processes in the Southern Ocean have a global reach, and paleoceanographic reconstructions from this region provide crucial constraints on the links between ocean circulation dynamics, deep water chemistry, and climate change (e.g. Robinson and van de Flierdt, 2009; Burke and Robinson, 2012; Roberts et al., 2016; Rae et al., 2018).

In the modern ocean, there are two main overturning circulation cells: an upper cell with deep water formation in the North Atlantic (i.e., North Atlantic Deep Water, NADW) and a lower cell in which deep waters form in the Southern Ocean (i.e., Antarctic Bottom Water, AABW). These two cells are interconnected (Talley, 2013), because NADW is exported at mid-depths into the Southern Ocean, where it is incorporated into Lower Circumpolar Deep Water (LCDW) which feeds AABW formation (Fig. 1b). After ventilating the deep Indian and Pacific Oceans, those southern-sourced waters flow back into recirculating Upper Circumpolar Deep Water (UCDW), which upwells in the Southern Ocean and is exported northwards at intermediate depths, thereby resupplying the upper cell (Talley, 2013). Since the upper and lower overturning cells are connected through upwelling and mixing in the Southern Ocean, the properties of NADW and AABW are exchanged between the two cells and the modern deep ocean is relatively homogeneous.

However, this picture likely differed significantly in the past, with changes in the deep southern-sourced overturning cell being a leading candidate to explain late Pleistocene glacial-interglacial atmospheric CO_2 variability (Toggweiler, 1999; Anderson et al., 2009; Sigman et al., 2010; Skinner et al., 2010; Burke and Robinson, 2012; Roberts et al., 2016; Rae et al., 2018). Physical mechanisms that could have enhanced glacial carbon sequestration in the lower cell include reduced overturning rates (Toggweiler, 1999), increased isolation from the atmosphere (Keeling and Stephens, 2001), or an increase in its volumetric contribution to the global ocean (Skinner, 2009). Recently, reduced mixing between the upper and lower cells has been proposed as the key mechanism for deep ocean carbon storage (Lund et al., 2011), leading to a renewed focus on the role of sea-ice in controlling Southern Ocean buoyancy and stratification (Ferrari et al., 2014; Nadeau et al., 2019). However, diagnosing the importance of any of these mechanisms for the carbon cycle is challenging because neither data nor models agree on the nature of the glacial lower cell circulation (e.g. Bőhm et al., 2015; Kurahashi-Nakamura et al., 2017; Du et al., 2018; Hu and Piotrowski, 2018; Muglia et al., 2018).

A better understanding of past lower-cell dynamics requires evidence on deglacial changes within the Southern Ocean, where the challenges of strong flow speeds and poor foraminiferal preservation can be overcome using absolute-dated deep-sea corals as an archive of seawater chemistry (Robinson et al., 2014). Recent studies on fossil corals from the Drake Passage indicate that a poorly-ventilated, low-pH water mass occupied LCDW depths during the late glacial period (Burke and Robinson, 2012; Rae et al., 2018) and that its subsequent ventilation released carbon to the upper ocean and atmosphere towards the end of Heinrich Stadial 1 (Burke and Robinson, 2012; Martínez-Botí et al., 2015; Rae et al., 2018). However, a comprehensive interpretation of such changes in deep water chemistry requires independent constraints on water mass sourcing. Neodymium (Nd) isotopes have the potential to provide insights into water mass sources to the Southern Ocean because Atlantic and Pacific-derived waters have contrasting Nd isotopic compositions (Carter et al., 2012; van de Flierdt et al., 2016; Struve et al., 2017) and past compositions can be reliably recovered from deep-sea corals (van de Flierdt et al., 2010; Struve et al., 2017). To date, direct evidence for deglacial Nd isotopic compositions in the Drake Passage comes from only a single coral at UCDW depths (Robinson and van de Flierdt, 2009), with no data constraining the composition of the glacial lower cell within the ACC.

To fill this important gap, we present the first late glacial and deglacial neodymium (Nd) isotope record measured on a collection of deep-sea corals from modern LCDW depths in the Drake Passage. Our data constrain the proportions of Nd sourced from Atlantic versus Pacific waters in the Southern Ocean lower cell through time, and enable a multi-tracer comparison of Nd isotopes, radiocarbon, and boron isotopes measured on the same specimens (Burke and Robinson, 2012; Chen et al., 2015; Rae et al., 2018). Together, these data allow us to (i) address the structure of the glacial deep ocean circulation; (ii) re-assess the sequence and timing of deglacial deep ocean circulation reorganisation in the Southern Ocean; and (iii) test the proposed control of Southern Ocean sea-ice changes on global ocean circulation structure (Ferrari et al., 2014; Nadeau et al., 2019).

2. Regional setting and samples

The Drake Passage is the bottleneck of the circumpolar flow regime, and as such it defines the ACC (Orsi et al., 1995) and contains all major Southern Ocean water masses (Sudre et al., 2011). The mid-depths are characterised by a mixture of Atlantic-derived deep waters and recirculating Pacific waters, with a greater proportion of NADW within LCDW, and more Pacific influence (marked by lower oxygen concentrations) within UCDW (Fig. 1b) (Rintoul et al., 2001). Those water masses upwell towards the south along sloping isopycnals, and at the surface they experience either negative buoyancy forcing and flow south to become part of the lower cell (i.e., AABW), or positive buoyancy forcing and flow north to become part of the

upper cell (i.e., Antarctic Intermediate Water, AAIW) (Rintoul et al., 2001; Ferrari et al., 2014). Because LCDW upwells near Antarctica, it predominantly feeds into AABW formation, whereas UCDW feeds into the formation of AAIW and Subantarctic Mode Water (SAMW) north of the Polar Front (Fig. 1b). The deepest depths of the Drake Passage contain AABW formed in the Weddell Sea, as well as Southeast Pacific Deepwater (SPDW) formed in the high-latitude southeast Pacific Ocean (Sudre et al., 2011) (Fig. 1b).

In this study, we analysed 40 glacial and deglacial samples from 31 individual fossil coral specimens collected from three locations in the Drake Passage during expeditions NBP0805 and NBP1103 on the *RV Nathaniel B. Palmer* (Fig. 1a). The specimens span narrow depth ranges of 1701-1750 m at Sars Seamount (north of the Polar Front; n = 10), 982-1196 m at Interim Seamount (south of the Polar Front; n = 8), and 806-823 m at Shackleton Fracture Zone (south of the Southern ACC Front; n = 13) (Fig. 1b). Despite their different water depths, these sample locations all currently sit within LCDW (defined by a neutral density of 28.0-28.2 kgm^{-3}; Sudre et al., 2011) (Fig. 1b), or in the case of Interim Seamount straddle the boundary between LCDW and UCDW. The majority of specimens analysed were *Desmophyllum dianthus* (n = 27), supplemented by data from *Caryophyllia spp.* (n = 1) and *Paraconotrochus antarcticus* (n = 3). In the present day, UCDW and LCDW have fairly uniform Nd isotopic compositions at the coral sampling locations (ε_{Nd} = -8.2 ± 0.5, 2SD) (Struve et al., 2017) that reflect the balance of Atlantic (ε_{Nd} ~-13) and Pacific (ε_{Nd} ~-4) waters in the Southern Ocean (van de Flierdt et al., 2016). The homogeneity of Nd isotopes in the modern Southern Ocean reflects the smaller Nd isotope gradient between these water masses where they enter the Southern Ocean, as well as strong diapycnal mixing within the ACC (Watson et al., 2013), although this situation may have differed in past climate states.

3. Methods

Most of the coral sample ages were determined by uranium-thorium dating in recent studies (Burke and Robinson, 2012; Chen et al., 2015), while additional samples were dated at the University of Bristol following the method of Chen et al. (2015) (Supplementary Table S1). Typical age uncertainties are ~100-200 years (2σ) for glacial and deglacial aged samples, although five samples with higher initial ^{232}Th concentrations (>2 ng/g) have larger age uncertainties (> 500 years).

Neodymium isotopes were measured on chemistry cuts of the same subsampled portions of coral that were analysed for uranium-thorium dating and therefore correspond exactly to those ages (see Struve et al., 2016 for details). Neodymium isotope analyses were conducted by thermal ionisation mass spectrometry (TIMS) or multi-collector inductively-coupled plasma mass spectrometry (MC-ICP-MS) in the MAGIC laboratories at Imperial College London. For full analytical methods, see Struve et al. (2020). Based on analyses of in-house coral and USGS

151 BCR-2 rock reference materials, long term reproducibility was ~0.2-0.3 ε_{Nd} units. Data are
152 reported for all samples in Supplementary Table S1. In presenting the data, we focus on 35
153 samples from 30 specimens with well-constrained ages, and do not include data from five
154 samples with age uncertainties > 500 years.

155   Considering typical deep-sea coral growth rates of ~0.5-2 mm/year (Adkins et al., 2004),
156 an individual measurement is expected to provide a snapshot of ocean chemistry integrated
157 over a few decades to a century. Both *D. dianthus* and C*aryophyllia spp.* reliably record
158 dissolved Nd isotopic compositions of ambient seawater in the Drake Passage (van de Flierdt
159 et al., 2010; Struve et al., 2017), providing strong confidence in coral-based reconstructions in
160 this setting.

161

162 **4. Results**

163

164   The Nd isotopic compositions of fossil deep-sea corals from the Drake Passage are shown
165 by seamount and by species in Figure 2. There is good agreement between two Holocene-aged
166 fossil corals at Sars Seamount (Struve et al., 2020) and the modern composition of CDW in the
167 Drake Passage (ε_{Nd} = -8.2 ± 0.5) (Fig. 2a), which is consistent with the reliable recovery of past
168 seawater Nd isotope signatures from coral aragonite (assuming the modern seawater
169 composition is representative of LCDW during the Holocene). In addition, deglacial data from
170 *P. antarcticus* (Fig. 2b), a species which is uncalibrated for Nd isotopes, are consistent with
171 results from similarly-aged samples of the calibrated species *D. dianthus* and *Caryophyllia spp.*
172 (van de Flierdt et al., 2010; Struve et al., 2017) (Fig. 2b), supporting the use of *P. antarcticus*
173 for paleo-reconstructions.

174   The glacial and deglacial data comprise measurements from three seamounts (Fig. 2a),
175 but we combine these datasets into a composite record representing LCDW in the Drake
176 Passage (Fig. 2b). Combining the records is supported by (i) the similar neutral density of
177 seawater at each of the sites in the modern ocean (Fig. 1b); (ii) the expectation that the slope
178 of the isopycnals has not changed significantly in the past (e.g. Ferrari et al., 2014); (iii) the
179 geographic proximity of the sites (Fig. 1a); and (iv) the consistency of the records where they
180 overlap (Fig. 2a). While Southern Ocean frontal positions and water mass boundaries may have
181 shifted in the past, changes in the central and southern Drake Passage region were likely
182 minimal (McCave et al., 2013). In any case, the samples were collected from the upper levels
183 of LCDW in the modern day (Fig. 1b), and would have remained within LCDW during any
184 northwards frontal shifts that may have characterised the colder intervals during the past 40 kyr
185 (Gersonde et al., 2005).

186   Our combined late glacial and deglacial LCDW record shows overall variability of 2.5
187 ε_{Nd} units, ranging from values of -5.9 to -8.4 (Fig. 2b). During the glacial period (18-39 ka BP;
188 hereafter ka), LCDW Nd isotopic compositions in the Drake Passage were between -5.9 and -

189　7.7, and therefore more radiogenic than modern CDW in this region (ε_{Nd} = -8.2 ± 0.5) (Struve

190　et al., 2017). The least radiogenic glacial values (ε_{Nd} = -7.3 to -7.7) were recorded from 26 to

191　39 ka, representing the latter portion of Marine Isotope Stage (MIS) 3. In contrast, the most

192　radiogenic values (ε_{Nd} = -5.9 to -6.7) were confined to an interval from 19 to 26 ka,

193　approximately representing the Last Glacial Maximum (LGM), although variability in this

194　interval was high and less radiogenic values (ε_{Nd} = -7.2 to -7.5) were also recorded. At the end

195　of the LGM, Nd isotopic compositions shifted at ~18-20 ka to reach values of -7.5 to -8.0

196　during Heinrich Stadial 1. Some rapid variability is recorded around the end of Heinrich Stadial

197　1, ranging from ε_{Nd} = -6.9 ± 0.4 at 15.2 ka to ε_{Nd} = -8.3 ± 0.2 at 14.7 ka. A return to more

198　radiogenic values up to ε_{Nd} = -7.3 ± 0.2 occurred within the Bølling-Allerød/Antarctic Cold

199　Reversal, before values became less radiogenic during the Younger Dryas and reached a

200　modern-like composition of ε_{Nd} = -8.4 ± 0.2 at 11.9 ka.

201

202　**5. Discussion**

203

204　**5.1 Reduced influence of NADW in the glacial Southern Ocean lower cell**

205

206　　　　Our coral-based Nd isotope data represents the first LCDW record from the Drake

207　Passage, so it is instructive to place it in context with existing lower cell Nd isotope records

208　from the wider region. Comparison to both the deep Cape Basin of the southeast Atlantic (cores

209　RC11-83/TNO57-21; 4.7/5.0 km water depth; Piotrowski et al., 2008; Piotrowski et al., 2012)

210　and the deep equatorial Indian Ocean (core SK129-CR2; 3.8 km water depth; Wilson et al.,

211　2015) reveals very similar absolute values and temporal evolution during the glacial period and

212　Heinrich Stadial 1 (Fig. 3c). Given the effects of bioturbation and sedimentation rates of ~2

213　cm/kyr for SK129-CR2 and ~15-20 cm/kyr for RC11-83/TNO57-21, those sediment core

214　records integrate seawater chemistry over multi-centennial to millennial timescales, whereas

215　the coral data should be sensitive to sub-centennial variability, if present. Indeed, there does

216　appear to be greater variability in the coral data than in those sediment core records from 18 to

217　22 ka, but overall the lower cell records from the Drake Passage, the Cape Basin, and the Indian

218　Ocean are similar (Fig. 3c). We therefore infer that all three sites were ventilated by a similar

219　water mass, presumably LCDW, throughout the glacial period and early deglaciation, and that

220　these Nd isotope records represent a circumpolar signal rather than recording local circulation

221　or input signals. Importantly, agreement between multiple locations argues against a significant

222　control by porewater processes (Du et al., 2016) or boundary exchange (Lacan and Jeandel,

223　2005), consistent with modern observations from the Southern Ocean which is characterised

224　by rapid advection (Carter et al., 2012; van de Flierdt et al., 2016). Persistent connectivity

225　between these locations supports inter-ocean exchange of deep waters via the Southern Ocean

226　during the glacial period (e.g. McCave et al., 2013; Lynch-Stieglitz et al., 2016).

227   Given the wide geographical extent of this water mass signal, we interpret the more
228   radiogenic Nd isotopic compositions of LCDW during the glacial (ε_{Nd} = -5.9 to -7.7) compared
229   to the Holocene and modern day (ε_{Nd} ~-8.2 ± 0.5) (Figs. 2b, 3c) as an increased contribution of
230   radiogenic Nd from Pacific waters at the expense of NADW (van de Flierdt et al., 2016). This
231   difference was most pronounced during the LGM, with four samples recording ε_{Nd} values of -
232   5.9 to -6.7 (Fig. 3c), indicating a significant reduction in the proportion of NADW-derived Nd
233   in the lower cell. This scenario could potentially arise from reduced NADW production and
234   export (assuming relatively unchanged Nd isotopic compositions and concentrations in
235   NADW), but there is strong evidence for persistent Atlantic meridional overturning circulation
236   during the glacial period, including the LGM (McManus et al., 2004; Bradtmiller et al., 2014;
237   Bőhm et al., 2015) (Fig. 3b). We therefore rule out volumetric changes in NADW production
238   as the controlling factor, and instead suggest that NADW incorporation into the lower cell was
239   reduced as a result of changes in water mass geometry. A reduced influence of NADW in the
240   global lower cell at the LGM provides strong support for a glacial circulation mode with greater
241   stratification and more isolated upper and lower overturning cells (Ferrari et al., 2014).
242   Enhanced glacial stratification would also be expected to maintain steeper vertical Nd isotope
243   gradients in the Southern Ocean, such that a circulation response that is sensitive to modest
244   sea-ice variability (WAIS Divide Project Members, 2013; Xiao et al., 2016) could potentially
245   explain the rapid temporal variability in Nd isotopes at the LGM (Fig. 2b).

246   Whereas our data support the operation of a glacial circulation mode at the LGM, the Nd
247   isotopic composition of LCDW recorded by coral samples from MIS 3 (ε_{Nd} = -7.5 to -7.7; Fig.
248   3c) was only slightly more radiogenic than modern values (ε_{Nd} ~-8.2 ± 0.5). This observation
249   suggests that NADW-derived Nd was still incorporated into the lower cell at times during MIS
250   3, consistent with the deep North Atlantic overturning inferred at these times (e.g. Bőhm et al.,
251   2015). For stadial intervals and MIS 4, the Cape Basin record suggests that a glacial Southern
252   Ocean circulation mode was in operation (Piotrowski et al., 2008), but as yet there are no Drake
253   Passage coral data to constrain interpretations before 40 ka.

254

5.2 Distinct local bottom water in the glacial southwest Atlantic Ocean

256

257   In contrast to the Drake Passage, deep Cape Basin, and Indian Ocean records, a South
258   Atlantic site on the Mid-Atlantic Ridge (core MD07-3076; 3.8 km water depth; Skinner et al.,
259   2013) records distinct Nd isotopic compositions, which are both more radiogenic (ε_{Nd} ~-5.5)
260   and less variable during the LGM and early Heinrich Stadial 1 (Fig. 3c). Howe et al. (2016)
261   also observed an east-west Nd isotope gradient in the deep South Atlantic at the LGM, with
262   radiogenic compositions in the southwest Atlantic (ε_{Nd} ~-5 in core RC15-94 at 3.8 km and core
263   RC12-267 at 4.1 km) but not in the southeast Atlantic (ε_{Nd} = -6.4 in core TN057-6 PC4 at 3.7
264   km). We therefore propose that MD07-3076 on the Mid-Atlantic Ridge was not connected

along the same flow path as those other sites, and was influenced by a different bottom water source with a radiogenic Nd isotopic composition.

During the LGM, AABW formation in the Weddell Sea was probably restricted by the expansion of grounded ice (Hillenbrand et al., 2014; Huang et al., 2020), although a glacial version of AABW could potentially have formed in open-ocean polynyas (Cheon and Gordon, 2019) or coastal polynyas along the West Antarctic Peninsula (Smith et al., 2010). In the latter case, interaction with the volcanogenic lithologies of that region (Struve et al., 2017) could have produced a variety of AABW with a more radiogenic Nd isotopic composition than its modern counterpart (ε_{Nd} ~-9; van de Flierdt et al., 2016). Assuming a flow path into the southwest Atlantic Ocean similar to modern AABW (Rintoul et al., 2001), such a water mass could have affected site MD07-3076 on the Mid-Atlantic Ridge without influencing the Drake Passage. For this mechanism to be correct, ice in the Weddell Sea must have remained grounded until at least ~17.5 ka (Fig. 3c). However, evidence for the timing of ice retreat in the Weddell Sea is inconclusive (Hillenbrand et al., 2014), with estimates ranging from ~19 to 20 ka (Smith et al., 2010) to ~14 to 15 ka (Weber et al., 2011; Golledge et al., 2014).

An alternative possibility is that the deep southwest Atlantic was influenced by a bottom water mass that formed in the South Pacific sector of the Southern Ocean and traversed the Drake Passage below the LCDW depths monitored by our corals. In the modern ocean, SPDW follows such a pathway (Sudre et al., 2011) (Fig. 1b). However, while SPDW has a relatively radiogenic Nd isotopic composition (ε_{Nd} ~-7) near its source region (Carter et al., 2012), it is not isotopically distinct from LCDW in the Drake Passage (Struve et al., 2017). For a glacial analogue of SPDW to have controlled the MD07-3076 record requires both a more radiogenic Nd isotopic composition for SPDW at the LGM and more efficient transport of this signal into the South Atlantic. A more radiogenic composition for SPDW seems feasible given the radiogenic Nd isotopic compositions on the modern Amundsen Sea shelves (Carter et al., 2012) and the greater isolation between Atlantic and Pacific overturning cells proposed for the LGM (Ferrari et al., 2014; Sikes et al., 2017). It is also supported by the Nd isotopic compositions of around -6 recorded during the glacial period in southeast Pacific cores E11-2 (3.1 km) and PS75/056 (3.6 km) (Basak et al., 2018).

The uniquely radiogenic Nd isotopic composition of the glacial deep water mass at MD07-3076 in comparison to other LCDW records (Fig. 3c) is also matched by larger radiocarbon age offsets from the atmosphere (B-Atm ~2700-3700 years; Skinner et al., 2013) in comparison to LCDW in the Drake Passage (B-Atm ~1700-2400 years; Burke and Robinson, 2012) and deep Cape Basin (B-Atm ~1200-2000 years; Barker et al., 2010). These extreme properties emphasise its distinct sourcing and could point towards radiocarbon-depleted Pacific waters (Skinner et al., 2017) in its source region. We therefore favour a localised origin in the southeast Pacific sector of the Southern Ocean, but future studies from this region will be required to test this idea.

5.3 Early deglacial Southern Ocean circulation changes linked to sea-ice retreat

A striking feature of our new LCDW record is the change at ~18-20 ka from highly radiogenic Nd isotopic compositions that characterise much of the LGM (-6 to -6.5) towards consistently less radiogenic compositions during Heinrich Stadial 1 (-7.5 to -8) (Fig. 3c), implying an increase in the proportion of Nd derived from NADW in the deep Southern Ocean. A deglacial shift towards unradiogenic values is also seen in other South Atlantic and Indian Ocean records (e.g. Piotrowski et al., 2008; Skinner et al., 2013; Wilson et al., 2015), and has often been interpreted in terms of strengthened NADW formation and its downstream advection. However, the Drake Passage changes occurred early in the deglaciation, coinciding with a weakening of Atlantic overturning circulation during Heinrich Stadial 1 (McManus et al., 2004; Bradtmiller et al., 2014; Bőhm et al., 2015) (Fig. 3b). Since the corals have absolute ages with uncertainties of only a few hundred years, it is a robust observation that the early deglacial shift in the Drake Passage precedes the strengthening and deepening of Atlantic overturning at the onset of the Bølling-Allerod (McManus et al., 2004; Barker et al., 2010). The Drake Passage changes also precede deglacial Nd isotope changes in the North Atlantic region (Bőhm et al., 2015; Zhao et al., 2019) so cannot be attributed to changes in the Nd isotopic composition of NADW, while the Pacific Nd isotopic composition appears to have been approximately constant between the LGM and Holocene (Hu et al., 2016). Therefore, it appears that Southern Ocean processes may have increased the incorporation of unradiogenic Nd from NADW into the lower cell at this time, despite reduced NADW production.

In Figure 4, we compare the Drake Passage Nd isotope record to ice-core reconstructions of regional temperature and sea-ice extent. The WAIS Divide Core records both an early interval of deglacial warming from ~18 to 22 ka (arrow on Fig. 4f), linked to regional insolation forcing (WAIS Divide Project Members, 2013), as well as a major warming event within Heinrich Stadial 1 (orange bar on Fig. 4). The early warming coincided with a rapid decrease in sea-salt sodium concentrations at ~19-20 ka (Fig. 4d), interpreted to record winter sea-ice retreat and reduction of the sea-ice zone (WAIS Divide Project Members, 2013), with a second rapid decrease at around ~17.5 ka within early Heinrich Stadial 1. Therefore, the radiogenic Nd isotopic compositions of LCDW during the LGM occurred within an interval of extended sea-ice, while the shift towards unradiogenic compositions at ~18-20 ka coincided with local warming and reduced sea-ice extent (Fig. 4). Reconstructions of sea-ice extent based on diatom abundance in sediment cores also indicate early deglacial warming and sea-ice retreat at ~19 ka in the southwest Atlantic (Allen et al., 2005; Xiao et al., 2016), southeast Atlantic (Shemesh et al., 2002), and Indo-Pacific sectors (Crosta et al., 2004).

Taken together, both the ice core and marine records indicate a link between increased glacial sea-ice extent and reduced NADW incorporation into the lower cell, which supports

hypotheses of a sea-ice control on ocean structure (Ferrari et al., 2014; Nadeau et al., 2019). According to Ferrari et al. (2014), the position of the summer sea-ice edge approximates the boundary between positive and negative buoyancy forcing, such that extended sea-ice would shoal the boundary between the upper and lower cells and reduce diapycnal mixing by rough seafloor bathymetry, ultimately decreasing NADW incorporation into the lower cell. Alternatively, Nadeau et al. (2019) emphasise that increased sea-ice production rates (independent of latitudinal extent) would increase the density of the lower cell, thereby stratifying the deep ocean and shoaling the northern-sourced branch of the upper cell. Our evidence for a link between deglacial sea-ice retreat and deep ocean circulation changes (Fig. 4) is consistent with the operation of either, or both, of these mechanisms. It is challenging to distinguish between the mechanisms because of the difficulty constraining both summer and winter sea-ice extent and sea-ice production in the past. However, one possibility is that deep ocean circulation changes occurred early in the deglacial sequence, responding sensitively to sea-ice changes forced by regional insolation (Fig. 4c,d), whereas increased surface upwelling and CO_2 outgassing during Heinrich Stadial 1 (Anderson et al., 2009; Martínez-Botí et al., 2015) may have required more extensive summer sea-ice retreat (Fig. 4d,e).

The key message here is that early deglacial changes in deep ocean structure appear to have been controlled by a reduction in Antarctic sea-ice, allowing increased admixture of NADW into LCDW, despite reduced Atlantic overturning during Heinrich Stadial 1. A recent study in the South Pacific also proposed early deglacial changes in deep Southern Ocean stratification during Heinrich Stadial 1 (Basak et al., 2018). While both studies indicate early deglacial Southern Ocean changes, our study differs in three significant ways. First, absolute dating of the corals provides robust confirmation that major circulation changes occurred before or during early Heinrich Stadial 1 (Fig. 4c). Second, the Drake Passage is well located to monitor a representative global LCDW signature, whereas the cores of Basak et al. (2018) were located at the northern edge of the ACC and may have been locally influenced by the incorporation of Pacific waters. Third, Nd isotope values of -7.5 to -8 for LCDW during Heinrich Stadial 1 (Fig. 4c) are too unradiogenic to originate in the Pacific sector (Basak et al., 2018), which implies that circumpolar incorporation of NADW was required. We cannot completely exclude that the changes in the Drake Passage could be related to an early deglacial onset of AABW production in the Weddell Sea region, but this possibility seems unlikely because an early shift is not observed in South Atlantic core MD07-3076 (Fig. 3c).

5.4 Onset of the modern Southern Ocean structure and impact of the Antarctic Cold Reversal

During late Heinrich Stadial 1, the Nd isotopic composition of LCDW in both the Drake Passage and the Cape Basin was around -7.5 to -8 (Fig. 3c), suggesting that the Southern Ocean

379 circulation was approaching the modern regime. The southern-sourced deep waters at Mid-
380 Atlantic Ridge site MD07-3076 also became less radiogenic, leading to a diminished gradient
381 between MD07-3076 and the LCDW corals by the end of Heinrich Stadial 1 (Fig. 3c). The
382 emergence of more homogeneous Nd isotope signatures in the deep Southern Ocean around
383 the Heinrich Stadial 1 to Bølling-Allerød transition is consistent with the timing of Southern
384 Ocean de-stratification inferred from radiocarbon (Burke and Robinson, 2012).

385 However, this transition towards a modern-like state was interrupted by a shift back
386 towards a more radiogenic Nd isotopic composition for LCDW of -7.3 ± 0.2 at 14.1 ka, closely
387 following the trend of the Antarctic Cold Reversal (Fig. 3c,d). More radiogenic values at this
388 time seem surprising, given that NADW production during the Bølling-Allerød was strong and
389 deep (McManus et al., 2004; Piotrowski et al., 2008; Barker et al., 2010) (Fig. 3b). However,
390 Southern Ocean cooling and sea-ice expansion during the Antarctic Cold Reversal (Fig. 4d,f)
391 could have shoaled the boundary between the upper and lower cells, once again reducing the
392 incorporation of NADW into the lower cell. Unlike the LGM, the changes during the Antarctic
393 Cold Reversal were short-lived and less extreme, with the Nd isotopic composition of LCDW
394 returning to unradiogenic values by the Younger Dryas (ε_{Nd} ~-7.8 to -8.4) (Fig. 3c), indicating
395 renewed mixing and establishment of a modern-like circulation mode at this time.

396 In the South Pacific, Basak et al. (2018) proposed that the deglacial transition towards a
397 modern-like Southern Ocean circulation structure had two steps, during Heinrich Stadial 1 and
398 the Younger Dryas, while benthic carbon isotope records from near New Zealand indicate more
399 gradual changes starting before Heinrich Stadial 1 and continuing until the early Holocene
400 (Clementi et al., 2019). Our observations of early deglacial changes, a transient shift towards a
401 modern-like ocean structure by the end of Heinrich Stadial 1, and a permanent recovery
402 towards modern Nd isotopic compositions after the Antarctic Cold Reversal, are broadly
403 consistent with these studies. In particular, the link with Antarctic climate evolution emphasises
404 the importance of Southern Ocean processes (Fig. 4) over NADW production (Fig. 3b) for
405 setting the chemistry of the global lower cell. However, future research will be required to
406 explore whether the more abrupt deglacial changes in the Drake Passage versus more protracted
407 changes in the Pacific Ocean reflect a difference of resolution between sediment core and coral
408 records, or regional differences between these settings.

409

410 **5.5 Establishment of the Holocene Atlantic circulation mode**

411

412 We demonstrated above that the deep Cape Basin was ventilated by LCDW during the
413 glacial period and Heinrich Stadial 1, with its Nd isotopic composition tracking LCDW in the
414 Drake Passage (Section 5.1). In contrast, during the Holocene, the deep Cape Basin is offset
415 by 1-2 ε_{Nd} units towards a less radiogenic Nd isotopic composition than LCDW (Fig. 3c), which
416 reflects a contribution of NADW to that basin. Comparing those two records reveals that this

modern gradient first emerged during the Bølling-Allerød/Antarctic Cold Reversal, when the deep Cape Basin became increasingly unradiogenic while LCDW in the Drake Passage returned to more radiogenic values (Fig. 3c). We attribute this change to a southward extension and/or deepening of the unradiogenic tongue of NADW, forming a mixing zone between NADW and LCDW in the deep Cape Basin. By constraining the composition of LCDW, our data supports the emergence of a modern-like Atlantic circulation in this region at the Bølling-Allerød transition, strengthening previous inferences from individual proxy records (Piotrowski et al., 2008; Barker et al., 2010).

In contrast, comparing the Nd isotope record from Mid-Atlantic Ridge site MD07-3076 (Skinner et al., 2013) to the Drake Passage coral record suggests a later onset for a modern-like circulation pattern in the southwest Atlantic Ocean. During the LGM and Heinrich Stadial 1, MD07-3076 was ventilated by a distinct water mass with a more radiogenic Nd isotopic composition than LCDW (Section 5.2), whereas its composition during the Bølling-Allerød and Younger Dryas matched the Drake Passage corals (Fig. 3c). Therefore, while a change of water mass origin at MD07-3076 did occur at the onset of the Bølling-Allerød, we infer that it was still ventilated by southern-sourced waters, which supports the interpretation of improved ventilation of southern-sourced waters during Heinrich Stadial 1 and the Bølling-Allerød (Skinner et al., 2013). The MD07-3076 record only diverges from the Drake Passage record during the early Holocene, indicating the arrival of unradiogenic NADW in the southwest Atlantic at this time (Fig. 3c).

The earlier deglacial return of NADW to the deep Cape Basin (Bølling-Allerød) than to the Mid-Atlantic Ridge (early Holocene) (Fig. 3c) appears to reflect their positions with respect to the flow paths of NADW and AABW. In the modern ocean, the main export pathway for NADW is via the southeast Atlantic, whereas AABW inflow is more important in the southwest Atlantic where it flows northwards in a deep western boundary current (Rintoul et al., 2001). Therefore, the later return of NADW to site MD07-3076 could indicate a delay in establishing a full-strength Holocene Atlantic circulation mode, with NADW reaching the deep Cape Basin but not MD07-3076 during the Bølling-Allerød, consistent with model results (Barker et al., 2010). The dynamics of southern-sourced water formation may also have contributed to this spatial asynchrony, with extremely dense waters at MD07-3076 during both the glacial period and deglaciation (Roberts et al., 2016) restricting the penetration of NADW into the deep western basin. In support of that idea, the early Holocene return of NADW to MD07-3076 inferred from Nd isotope gradients (Fig. 3c) coincides with a switch to less dense waters at MD07-3076 (Roberts et al., 2016).

5.6 Relationship between lower cell circulation, chemistry, and carbon storage

454   In this final section, we explore the carbon cycle implications of the lower cell circulation
455   changes, using a multi-proxy comparison of Nd isotopes, radiocarbon, and boron isotopes. All
456   three tracers record significant glacial-interglacial changes in LCDW, with the most extreme
457   values during the LGM (Fig. 4a-c). Ventilation ages (B-Atm) during the LGM were ~1700-
458   2400 years (Burke and Robinson, 2012; Chen et al., 2015), up to double those in modern
459   LCDW, and boron isotope values indicate low-pH conditions (Rae et al., 2018). Hence, to first
460   order, a reduced NADW contribution to the lower cell was linked to greater isolation from the
461   atmosphere and enhanced carbon storage. Given the low atmospheric CO_2 concentrations
462   during the LGM (~185-195 ppm; Fig. 4e), our Nd isotope data are consistent with a role for
463   ocean circulation changes in carbon drawdown, in particular supporting hypotheses that sea-
464   ice expansion enhanced deep ocean stratification and restricted connectivity between upper and
465   lower cells (Ferrari et al., 2014; Nadeau et al., 2019; Stein et al., 2020). A reduced proportion
466   of Atlantic-sourced waters in LCDW at the LGM is also consistent with a ventilation volume
467   hypothesis (Skinner, 2009). During MIS 3, atmospheric CO_2 concentrations were also low
468   (~200-215 ppm; Fig. 4e) whereas water mass sourcing in LCDW appears to have been quite
469   similar to modern (Fig. 4c), which supports a maximum direct contribution of water mass
470   source changes to CO_2 drawdown of a few tens of ppm (Hain et al., 2010). Our inference of
471   similar water mass sourcing between MIS 3 and the Holocene, together with the coupled
472   variability in Nd isotopes and radiocarbon during the LGM (Fig. 5), also suggests that ocean
473   circulation and stratification may be more sensitive to glacial sea-ice dynamics than indicated
474   in current models (Stein et al., 2020).
475   Interestingly, when considering the transitions into and out of the LGM in detail, the co-
476   variation among these tracers breaks down. The excursion to poorly-ventilated, low-pH waters
477   at ~27 ka preceded the reduction in the NADW contribution inferred from Nd isotopes (Fig.
478   4a-c), while the pH and ventilation did not change significantly with the increased contribution
479   of Atlantic-sourced waters at ~18-20 ka. Decoupling between these tracers is a robust
480   observation because measurements were made on the same specimens, which only allows
481   offsets of up to ~100 years. This relationship is highlighted in a cross-plot of ventilation ages
482   against Nd isotopes (Fig. 5a), with covariation along gentle slopes indicating water mass
483   mixing, in contrast to steep jumps between 35 and 27 ka and at ~15.4 ka which indicate major
484   changes in ventilation. While it is challenging to separate changes in deep ocean residence
485   times from changes in ocean-atmosphere exchange in deep water formation regions, it is clear
486   that LGM radiocarbon ages in LCDW were at least ~600 years older than would be predicted
487   from the modern water mass mixing relationship (Fig. 5). This finding is important because it
488   indicates that large changes in carbon storage (inferred from radiocarbon and boron isotopes)
489   can occur independent of water mass sourcing, supporting a process control on carbon storage
490   and release from the lower cell (Rae et al., 2018).

491   The decoupling of tracers at the onset and end of the LGM also provides insights into
492 how such transient events may have operated. Notably, reduced ventilation and a decrease in
493 pH is recorded in a coral with unradiogenic Nd isotopes at 27.2 ka (Figs. 4, 5), which points to
494 the incorporation or 'trapping' of NADW within the lower cell during initial sea-ice advance,
495 as predicted by Ferrari et al. (2014). The incorporation of northern-ventilated waters with low
496 preformed nutrient contents into the southern-sourced lower cell would also have enhanced the
497 CO_2 drawdown capacity (Hain et al., 2010). As the lower cell became isolated from Atlantic
498 waters, it would be expected to have acquired Nd isotope properties reflecting radiogenic Nd
499 sources in the deep Pacific Ocean (Hu et al., 2016; Du et al., 2018), which is indeed seen in the
500 radiogenic Nd isotopic compositions of subsequent LGM corals (Fig. 4c) and in coupled trends
501 towards older radiocarbon ages (Fig. 5a).

502   At the end of the LGM, the Nd isotope shift in LCDW corals at ~18-20 ka preceded the
503 major step in both ventilation and pH near the end of Heinrich Stadial 1 (Figs. 4, 5). While the
504 replacement of Indo-Pacific deep waters with Atlantic waters by early Heinrich Stadial 1
505 appears to reflect a high sensitivity of deep ocean circulation to sea-ice changes (Fig. 4c,d),
506 this change preceded the deglacial CO_2 rise (Fig. 4e). The coincidence of poor ventilation and
507 low-pH conditions with unradiogenic Nd isotopes could indicate that the Atlantic waters
508 influencing the lower cell during early Heinrich Stadial 1 were themselves aged and carbon-
509 rich, consistent with glacial carbon storage in the Atlantic Ocean (e.g. Yu et al., 2016; Skinner
510 et al., 2017). However, in this case, the evasion of CO_2 that might be expected to have coincided
511 with a reduction in deep stratification must have been hindered by a remaining summer sea-ice
512 barrier (Keeling and Stephens, 2001) and/or misaligned Southern Hemisphere westerly winds
513 that limited near-surface upwelling (Anderson et al., 2009). Such temporal decoupling hints at
514 differing roles for sea-ice and westerly winds in the deglacial climate sequence. Whereas the
515 upper cell circulation in the Drake Passage appears to be sensitive to westerly wind forcing
516 during the Holocene (Struve et al., 2020), the limited evidence from LCDW depths provides
517 no indication of wind-driven Holocene variability in the lower cell (Fig. 2b). However, future
518 studies should explore the potential for coupled interactions between the sea-ice, ocean
519 circulation, and westerly winds during the last glacial cycle.

520

521 **6. Conclusions**

522

523   This study provides the first direct constraints from the Drake Passage on glacial and
524 deglacial water mass sourcing in LCDW, with implications for ocean circulation dynamics and
525 carbon storage on glacial-interglacial and millennial timescales. Using Nd isotopes to trace the
526 balance of unradiogenic Atlantic and radiogenic Pacific waters, we demonstrate a significant
527 reduction in the contribution of NADW to the lower cell during the LGM, and an early
528 deglacial shift towards an increased Atlantic component during Heinrich Stadial 1. These

changes were closely linked to Southern Ocean climate and sea-ice controls, supporting an emerging hypothesis that increased sea-ice extent and/or sea-ice production can shoal the boundary between upper and lower overturning cells and stratify the deep ocean (Ferrari et al., 2014; Nadeau et al., 2019). We infer ongoing incorporation of NADW into the lower cell during Heinrich Stadial 1 and the Younger Dryas, but reduced NADW proportions during the Bølling-Allerød/Antarctic Cold Reversal, which provides a clear demonstration that Southern Ocean structure (rather than Atlantic overturning strength) is the dominant control on water mass sourcing in the deep Southern Ocean. Finally, we emphasise that our evidence on LCDW composition in the Drake Passage provides new constraints on water mass sourcing in other ocean basins and indicates a spatially asynchronous deglacial return of NADW to the deep south Atlantic Ocean.

Acknowledgments

Figures

554
555
Fig. 1: Location map and hydrographic section across the Drake Passage. (a) Location of the Drake Passage coral samples and South Atlantic sediment cores from the Cape Basin (RC11-83/TNO57-21; Piotrowski et al., 2008; Piotrowski et al., 2012) and Mid-Atlantic Ridge (MD07-3076; Skinner et al., 2013). Also shown are mean positions of the surface fronts of the ACC (Orsi et al., 1995): SAF, Subantarctic Front; PF, Polar Front; SACC, Southern ACC Front. SFZ, Shackleton Fracture Zone. (b) Section across the Drake Passage showing oxygen in ml/l (coloured; Garcia et al., 2014), neutral density anomaly in kgm^{-3} (black contour lines; Jackett and McDougall, 1997), and sub-surface water masses (Rintoul et al., 2001; Sudre et al., 2011). AAIW, Antarctic Intermediate Water; UCDW, Upper Circumpolar Deep Water; LCDW, Lower Circumpolar Deep Water; SPDW, Southeast Pacific Deep Water; AABW, Antarctic Bottom Water.
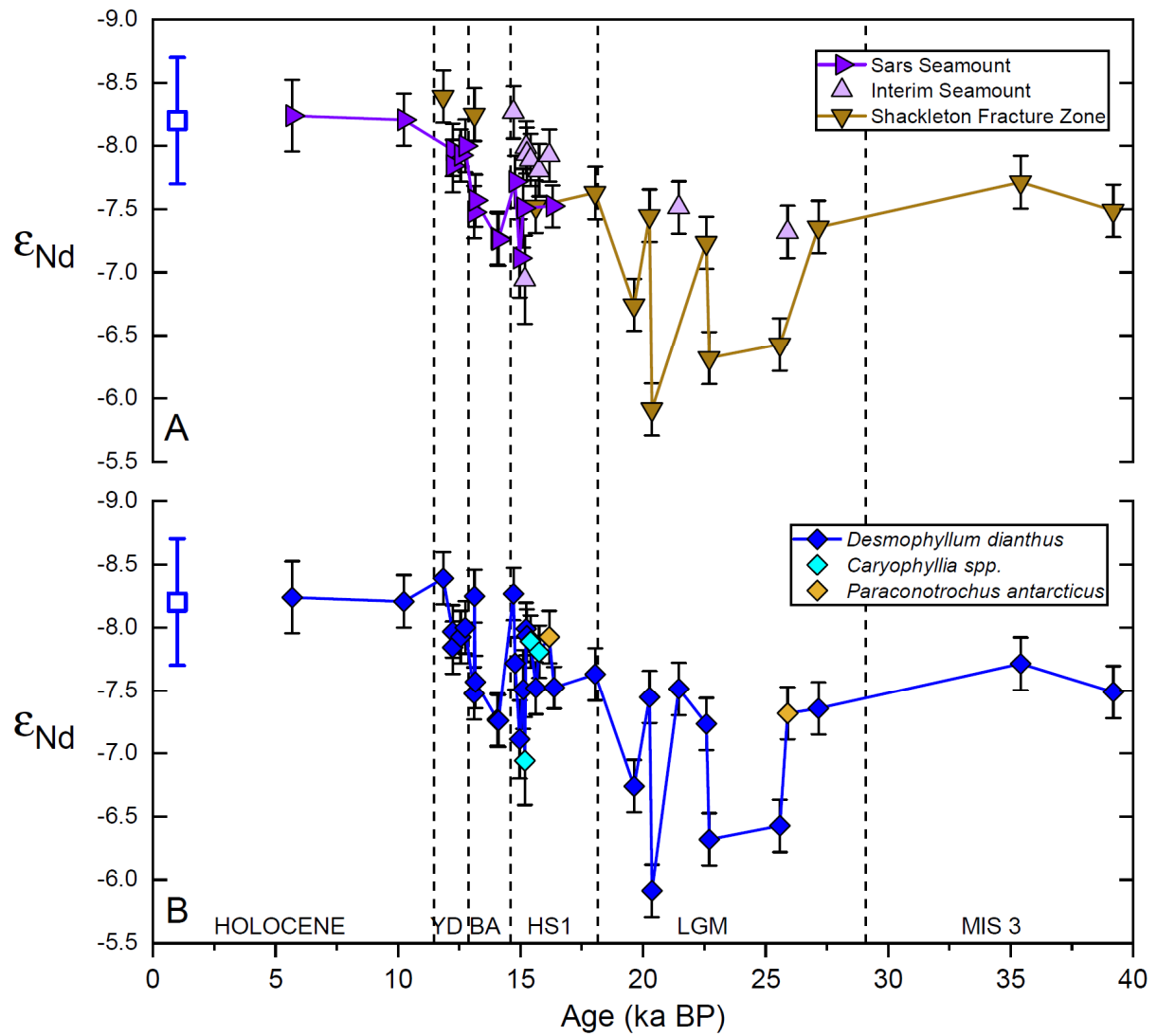
Fig. 2: Drake Passage coral Nd isotope data from 0 to 40 ka. (a) Data by seamount plotted as symbols, with lines connecting the Sars Seamount data from 5.8 to 16.4 ka and the Shackleton Fracture Zone data from 15.6 to 39.2 ka. (b) Composite record of all coral data representing LCDW, with species distinguished by coloured symbols. The modern range of seawater compositions for CDW in the Drake Passage (mean and 2SD, n=15) is shown on both panels near the y-axis (open blue square; Struve et al., 2017). Uncertainties for Nd isotopes are 2σ. Uncertainties on ages are comparable to or smaller than the symbol size. YD, Younger Dryas; BA, Bølling-Allerød; HS1, Heinrich Stadial 1; LGM, Last Glacial Maximum; MIS 3, Marine Isotope Stage 3.
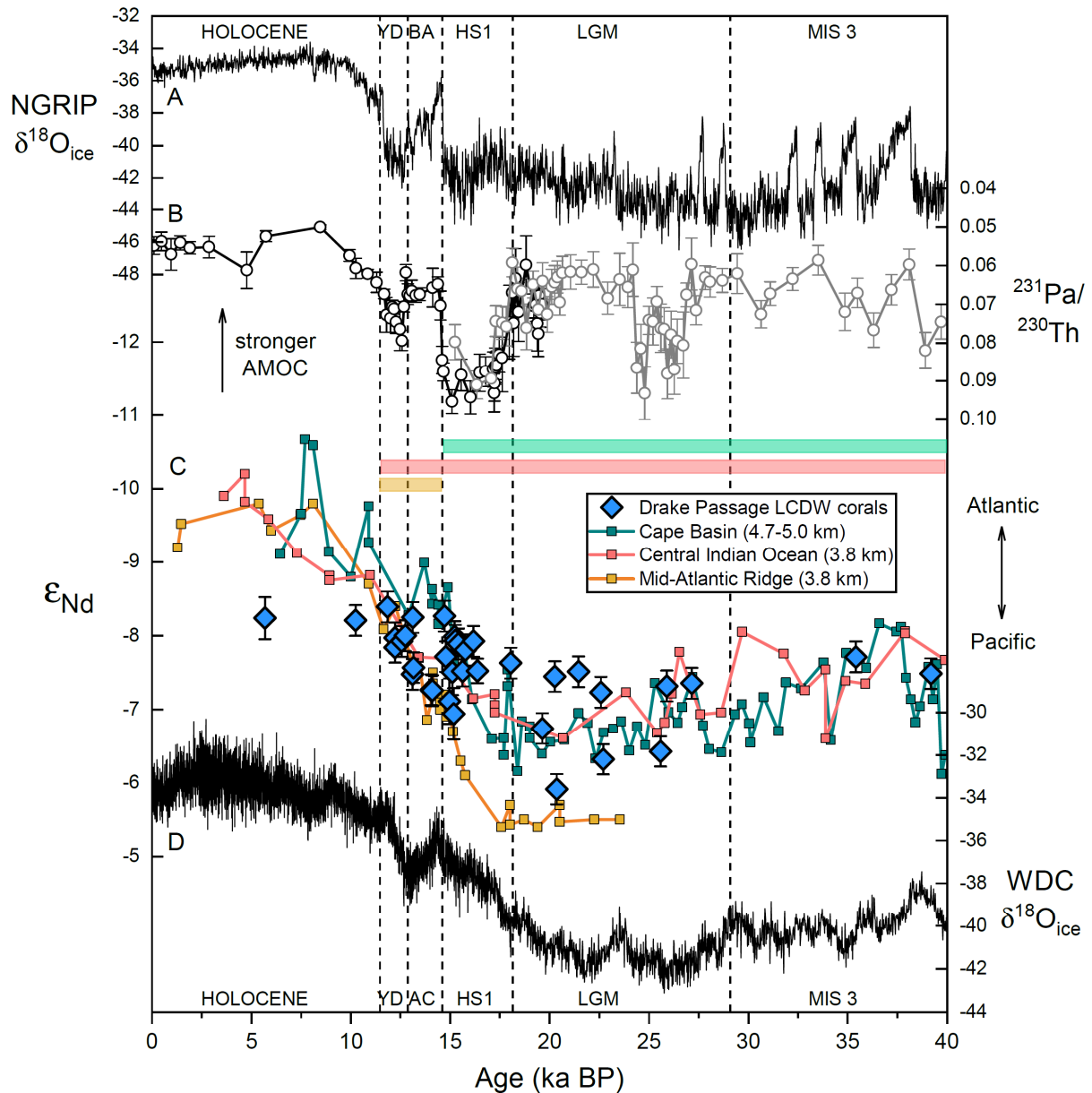
Fig. 3: Comparison of Drake Passage coral Nd isotopes to other lower cell Nd isotope records and Atlantic overturning reconstructions in a global climate context. (a) Greenland temperature proxy $\delta^{18}O_{ice}$ in NGRIP on the GICC05 chronology (NGRIP, 2004). (b) Proxy reconstruction of Atlantic meridional overturning circulation (AMOC) from $^{231}Pa/^{230}Th$ excess at the deep Bermuda Rise sites OCE326-GGC5/ODP1063 (black, McManus et al., 2004; grey, Bőhm et al., 2015). (c) Neodymium isotope records from Drake Passage LCDW corals, deep Cape Basin core RC11-83/TNO57-21 (foraminifera and sediment leachates; Piotrowski et al., 2008; Piotrowski et al., 2012), central Indian Ocean core SK129-CR2 (sediment leachates validated by foraminifera and fish teeth; Wilson et al., 2015), and Mid-Atlantic Ridge core MD07-3076 (foraminifera and fish teeth; Skinner et al., 2013). Uncertainties for coral Nd isotope data are 2σ, while uncertainties for coral ages are smaller than the symbol size. For clarity, uncertainties on the sediment core records are not shown. Horizontal bars highlight intervals when the Drake Passage corals match records from the Cape Basin (green bar), the central Indian Ocean (red bar), and the Mid-Atlantic Ridge (orange bar). (d) Antarctic temperature proxy $\delta^{18}O_{ice}$ in WAIS Divide Core (WDC; WAIS Divide Project Members, 2015). YD, Younger Dryas; BA, Bølling-Allerød; HS1, Heinrich Stadial 1; LGM, Last Glacial Maximum; MIS 3, Marine Isotope Stage 3; AC, Antarctic Cold Reversal.
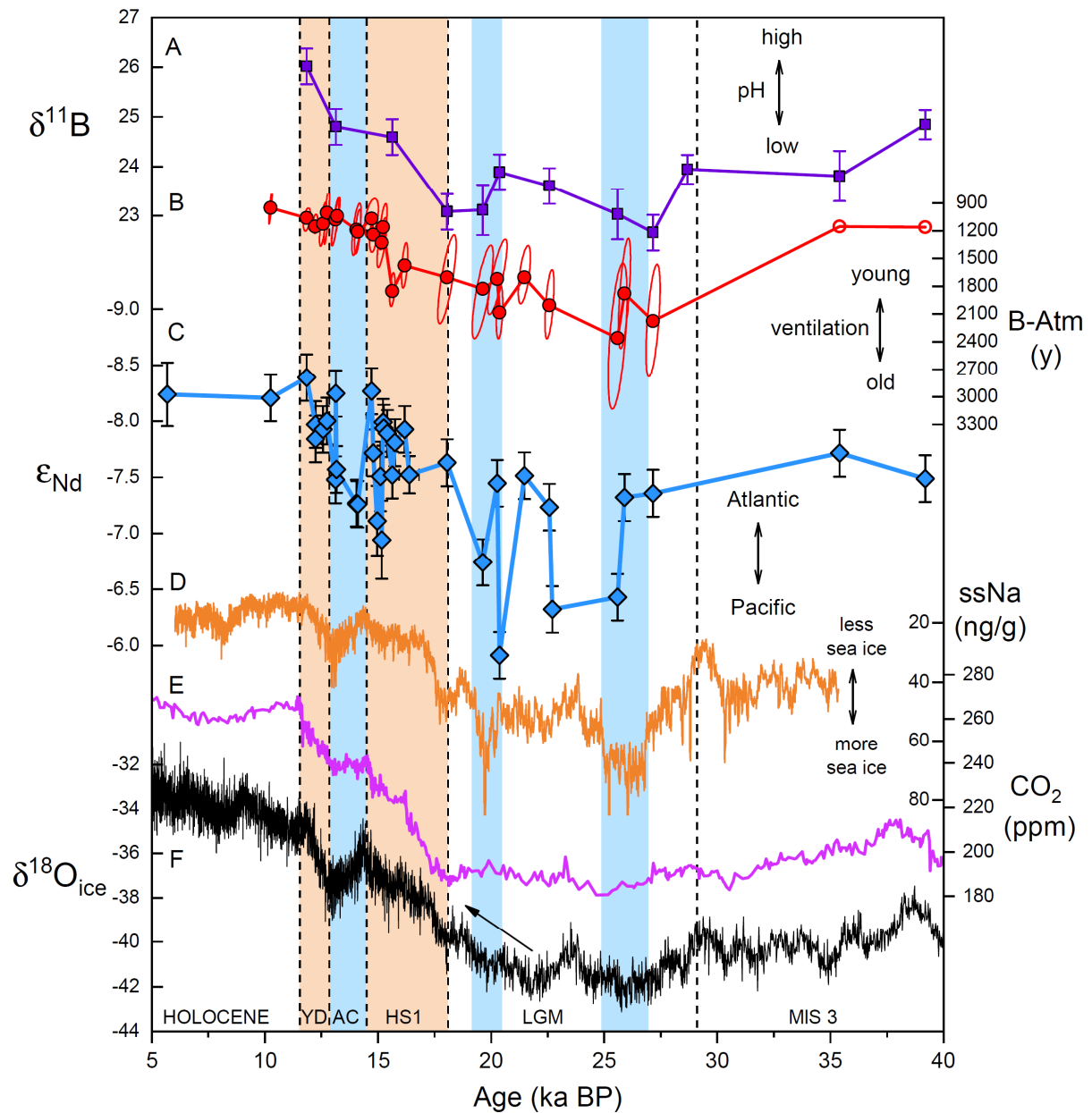
Fig. 4: Evolution of water mass sourcing and chemical properties of LCDW from 5 to 40 ka, based on Drake Passage deep-sea corals, compared to Southern Ocean climate records. (a) Deep water pH inferred from boron isotopes (Rae et al., 2018). (b) Deep water radiocarbon age offset from the contemporaneous atmosphere (B-Atm) (Burke and Robinson, 2012; Chen et al., 2015). Open symbols indicate two samples with large uncertainties in B-Atm and for clarity their error ellipses ($\pm$ ~2-2.5 kyr) are not shown. (c) Neodymium isotopes in LCDW corals (uncertainties for Nd isotopes are 2σ; uncertainties for ages are smaller than the symbol size). (d) Sea-salt sodium (ssNa, 15-point smoothed) in WAIS Divide Core as a proxy for sea-ice extent (WAIS Divide Project Members, 2015). (e) Atmospheric CO_2 compilation from Antarctic ice cores (Bereiter et al., 2015). (f) Antarctic temperature proxy $\delta^{18}O_{ice}$ in WAIS Divide Core (WAIS Divide Project Members, 2015), with arrow indicating early deglacial warming. Blue bars highlight the Antarctic Cold Reversal and two intervals during the LGM with particularly expanded sea-ice, which each correspond to shifts towards more radiogenic Nd isotopes. Orange bars highlight Antarctic warm intervals during the deglaciation. YD, Younger Dryas; AC, Antarctic Cold Reversal; HS1, Heinrich Stadial 1; LGM, Last Glacial Maximum; MIS 3, Marine Isotope Stage 3.

19
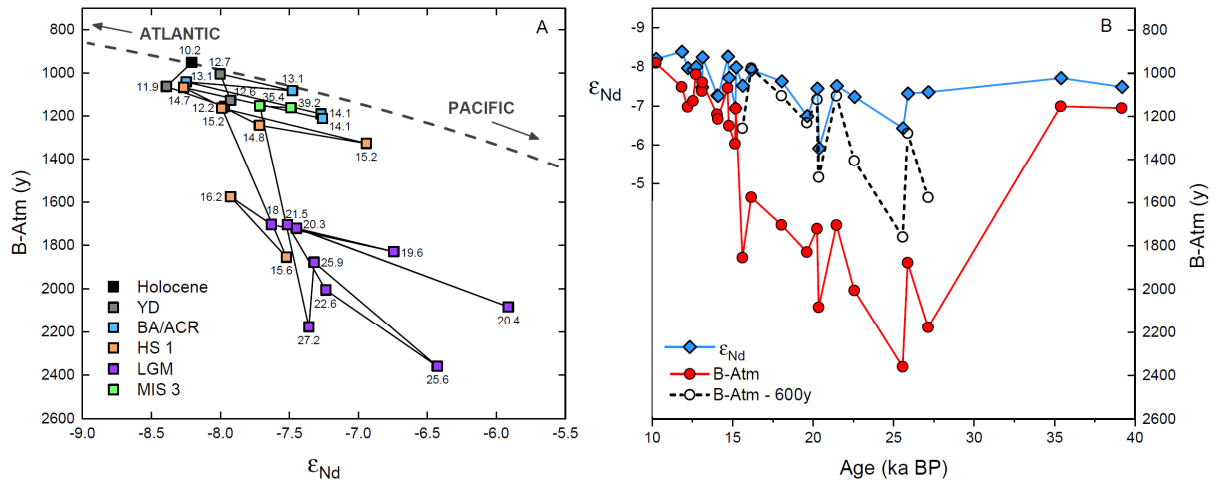
Fig. 5: Comparison of Nd isotopes and radiocarbon measured on the same LCDW coral specimens. (a) Cross-plot of Nd isotopes versus radiocarbon offset from the contemporaneous atmosphere (B-Atm). Data points are coloured by time interval and labelled with ages (ka), while consecutive data points are connected by lines as a guide to temporal trends (but note that the inferred age sequence may occasionally be incorrect where adjacent samples have overlapping age uncertainties). Modern mixing line between Atlantic (NADW) and Pacific (Pacific Deep Water) water masses is also shown for comparison, based on modern endmember Nd isotopic compositions and concentrations (dashed grey line; see Struve et al. 2020 for details). (b) Time series of Nd isotopes (blue diamonds) and radiocarbon offset from the contemporaneous atmosphere (B-Atm, red circles). Scaling of the two y-axes approximately follows the modern mixing line shown in (a). Also shown is a portion of the radiocarbon data from 15.6 to 27.2 ka with 600 years subtracted (black open circles and dashed line) to enable visual comparison with the Nd isotope record. For clarity, error bars are not shown on these plots (see Fig. 4).

References

Adkins, J.F., Henderson, G.M., Wang, S.L., O'Shea, S., Mokadem, F., 2004. Growth rates of the deep-sea scleractinia *Desmophyllum cristagalli* and *Enallopsammia rostrata*. Earth Planet. Sci. Lett. 227, 481-490.

Allen, C.S., Pike, J., Pudsey, C.J., Leventer, A., 2005. Submillennial variations in ocean conditions during deglaciation based on diatom assemblages from the southwest Atlantic. Paleoceanography 20, PA2012, doi:2010.1029/2004PA001055.

Anderson, R.F., Ali, S., Bradtmiller, L.I., Nielsen, S.H.H., Fleisher, M.Q., Anderson, B.E., Burckle, L.H., 2009. Wind-driven upwelling in the Southern Ocean and the deglacial rise in atmospheric CO_2. Science 323, 1443-1448.

Barker, S., Knorr, G., Vautravers, M.J., Diz, P., Skinner, L.C., 2010. Extreme deepening of the Atlantic overturning circulation during deglaciation. Nat. Geosci. 3, 567-571.

Basak, C., Fröllje, H., Lamy, F., Gersonde, R., Benz, V., Anderson, R.F., Molina-Kescher, M., Pahnke, K., 2018. Breakup of last glacial deep stratification in the South Pacific. Science 359, 900-904.

Bereiter, B., Eggleston, S., Schmitt, J., Nehrbass-Ahles, C., Stocker, T.F., Fischer, H., Kipfstuhl, S., Chappellaz, J., 2015. Revision of the EPICA Dome C CO2 record from 800 to 600 kyr before present. Geophys. Res. Lett. 42, 542-549.

Bőhm, E., Lippold, J., Gutjahr, M., Frank, M., Blaser, P., Antz, B., Fohlmeister, J., Frank, N., Andersen, M.B., Deininger, M., 2015. Strong and deep Atlantic meridional overturning circulation during the last glacial cycle. Nature 517, 73-76.

Bradtmiller, L.I., McManus, J.F., Robinson, L.F., 2014. [231]Pa/[230]Th evidence for a weakened but persistent Atlantic meridional overturning circulation during Heinrich Stadial 1. Nature Communications 5, 5817, doi: 5810.1038/ncomms6817.

Burke, A., Robinson, L.F., 2012. The Southern Ocean's role in carbon exchange during the last deglaciation. Science 335, 557-561.

Carter, P., Vance, D., Hillenbrand, C.D., Smith, J.A., Shoosmith, D.R., 2012. The neodymium isotopic composition of waters masses in the eastern Pacific sector of the Southern Ocean. Geochim. Cosmochim. Acta 79, 41-59.

Chen, T.Y., Robinson, L.F., Burke, A., Southon, J., Spooner, P., Morris, P.J., Ng, H.C., 2015. Synchronous centennial abrupt events in the ocean and atmosphere during the last deglaciation. Science 349, 1537-1541.

Cheon, W.G., Gordon, A.L., 2019. Open-ocean polynyas and deep convection in the Southern Ocean. Sci Rep 9, 6935, doi: 10.1038/s41598-019-43466-2

Clementi, V.J., Sikes, E.L., 2019. Southwest Pacific vertical structure influences on oceanic carbon storage since the Last Glacial Maximum. Paleoceanography and Paleoclimatology 34, 734-754.

Crosta, X., Sturm, A., Armand, L., Pichon, J.-J., 2004. Late Quaternary sea ice history in the Indian sector of the Southern Ocean as recorded by diatom assemblages. Mar. Micropaleontol. 50, 209-223.

Du, J., Haley, B.A., Mix, A.C., Walczak, M.H., Praetorius, S.K., 2018. Flushing of the deep Pacific Ocean and the deglacial rise of atmospheric CO2 concentrations. Nat. Geosci. 11, 749-755.

669 Du, J.H., Haley, B.A., Mix, A.C., 2016. Neodymium isotopes in authigenic phases, bottom waters and
670 detrital sediments in the Gulf of Alaska and their implications for paleo-circulation reconstruction.
671 Geochim. Cosmochim. Acta 193, 14-35.

672 Ferrari, R., Jansen, M.F., Adkins, J.F., Burke, A., Stewart, A.L., Thompson, A.F., 2014. Antarctic sea
673 ice control on ocean circulation in present and glacial climates. Proc. Natl. Acad. Sci. U.S.A. 111,
674 8753-8758.

675 Garcia, H.E., Locarnini, R.A., Boyer, T.P., Antonov, J.I., Baranova, O.K., Zweng, W.M., Reagan,
676 J.R., Johnson, D.R., 2014. World Ocean Atlas 2013, Volume 3: Dissolved Oxygen, Apparent Oxygen
677 Utilization, and Oxygen Saturation, in: Levitus, S. (Ed.), NOAA Atlas NESDIS 75.

678 Gersonde, R., Crosta, X., Abelmann, A., Armand, L., 2005. Sea-surface temperature and sea ice
679 distribution of the Southern Ocean at the EPILOG Last Glacial Maximum—a circum-Antarctic view
680 based on siliceous microfossil records. Quat. Sci. Rev. 24, 869-896.

681 Golledge, N.R., Menviel, L., Carter, L., Fogwill, C.J., England, M.H., Cortese, G., Levy, R.H., 2014.
682 Antarctic contribution to meltwater pulse 1A from reduced Southern Ocean overturning. Nature
683 Communications 5, 5107, doi: 10.1038/ncomms6107.

684 Hain, M.P., Sigman, D.M., Haug, G.H., 2010. Carbon dioxide effects of Antarctic stratification, North
685 Atlantic Intermediate Water formation, and subantarctic nutrient drawdown during the last ice age:
686 Diagnosis and synthesis in a geochemical box model. Glob. Biogeochem. Cycle 24, doi:
687 10.1029/2010gb003790.

688 Hillenbrand, C.-D., Bentley, M.J., Stolldorf, T.D., Hein, A.S., Kuhn, G., Graham, A.G.C., Fogwill,
689 C.J., Kristoffersen, Y., Smith, J.A., Anderson, J.B., Larter, R.D., Melles, M., Hodgson, D.A.,
690 Mulvaney, R., Sugden, D.E., 2014. Reconstruction of changes in the Weddell Sea sector of the
691 Antarctic Ice Sheet since the Last Glacial Maximum. Quat. Sci. Rev. 100, 111-136.

692 Howe, J.N.W., Piotrowski, A.M., Noble, T.L., Mulitza, S., Chiessi, C.M., Bayon, G., 2016. North
693 Atlantic Deep Water production during the Last Glacial Maximum. Nature Communications 7, 11765,
694 doi: 11710.11038/ncomms11765.

695 Hu, R., Piotrowski, A.M., 2018. Neodymium isotope evidence for glacial-interglacial variability of
696 deepwater transit time in the Pacific Ocean. Nature Communications 9, 4709, doi: 4710.1038/s41467-
697 41018-07079-z.

698 Hu, R., Piotrowski, A.M., Bostock, H.C., Crowhurst, S., Rennie, V., 2016. Variability of neodymium
699 isotopes associated with planktonic foraminifera in the Pacific Ocean during the Holocene and Last
700 Glacial Maximum. Earth Planet. Sci. Lett. 447, 130-138.

701 Huang, H., Gutjahr, M., Eisenhauer, A., Kuhn, G., 2020. No detectable Weddell Sea Antarctic Bottom
702 Water export during the Last and Penultimate Glacial Maximum. Nature Communications 11, 424,
703 doi: 10.1038/s41467-41020-14302-41463.

704 Jackett, D.R., McDougall, T.J., 1997. A neutral density variable for the world's oceans. Journal of
705 Physical Oceanography 27, 237-263.

706 Keeling, R.F., Stephens, B.B., 2001. Antarctic sea ice and the control of Pleistocene climate
707 instability. Paleoceanography 16, 112-131.

708 Kurahashi-Nakamura, T., Paul, A., Losch, M., 2017. Dynamical reconstruction of the global ocean
709 state during the Last Glacial Maximum. Paleoceanography 32, 326-350.

710   Lacan, F., Jeandel, C., 2005. Neodymium isotopes as a new tool for quantifying exchange fluxes at
711   the continent-ocean interface. Earth Planet. Sci. Lett. 232, 245-257.

712   Lund, D.C., Adkins, J.F., Ferrari, R., 2011. Abyssal Atlantic circulation during the Last Glacial
713   Maximum: Constraining the ratio between transport and vertical mixing. Paleoceanography 26, doi:
714   10.1029/2010pa001938.

715   Lynch-Stieglitz, J., Ito, T., Michel, E., 2016. Antarctic density stratification and the strength of the
716   circumpolar current during the Last Glacial Maximum. Paleoceanography 31, 539-552.

717   Martínez-Botí, M.A., Marino, G., Foster, G.L., Ziveri, P., Henehan, M.J., Rae, J.W.B., Mortyn, P.G.,
718   Vance, D., 2015. Boron isotope evidence for oceanic carbon dioxide leakage during the last
719   deglaciation. Nature 518, 219-222.

720   McCave, I.N., Crowhurst, S.J., Kuhn, G., Hillenbrand, C.D., Meredith, M.P., 2013. Minimal change
721   in Antarctic Circumpolar Current flow speed between the last glacial and Holocene. Nat. Geosci. 7,
722   113-116.

723   McManus, J.F., Francois, R., Gherardi, J.M., Keigwin, L.D., Brown-Leger, S., 2004. Collapse and
724   rapid resumption of Atlantic meridional circulation linked to deglacial climate changes. Nature 428,
725   834-837.

726   Muglia, J., Skinner, L.C., Schmittner, A., 2018. Weak overturning circulation and high Southern
727   Ocean nutrient utilization maximized glacial ocean carbon. Earth Planet. Sci. Lett. 496, 47-56.

728   Nadeau, L.-P., Ferrari, R., Jansen, M.F., 2019. Antarctic sea ice control on the depth of North Atlantic
729   Deep Water. J. Clim. 32, 2537-2551.

730   NGRIP, 2004. High-resolution record of Northern Hemisphere climate extending into the last
731   interglacial period. Nature 431, 147-151.

732   Orsi, A.H., Whitworth, T., Nowlin, W.D., 1995. On the meridional extent and fronts of the Antarctic
733   Circumpolar Current. Deep Sea Research Part I: Oceanographic Research Papers 42, 641-673.

734   Piotrowski, A.M., Galy, A., Nicholl, J.A.L., Roberts, N., Wilson, D.J., Clegg, J.A., Yu, J., 2012.
735   Reconstructing deglacial North and South Atlantic deep water sourcing using foraminiferal Nd
736   isotopes. Earth Planet. Sci. Lett. 357, 289-297.

737   Piotrowski, A.M., Goldstein, S.L., Hemming, S.R., Fairbanks, R.G., Zylberberg, D.R., 2008.
738   Oscillating glacial northern and southern deep water formation from combined neodymium and
739   carbon isotopes. Earth Planet. Sci. Lett. 272, 394-405.

740   Rae, J.W.B., Burke, A., Robinson, L.F., Adkins, J.F., Chen, T., Cole, C., Greenop, R., Li, T., Littley,
741   E.F.M., Nita, D.C., Stewart, J.A., Taylor, B.J., 2018. CO_2 storage and release in the deep Southern
742   Ocean on millennial to centennial timescales. Nature 562, 569-573.

743   Rintoul, S.R., Hughes, C.W., Olbers, D., 2001. The Antarctic Circumpolar Current system, in:
744   Siedler, G., Church, J., Gould, J. (Eds.), Ocean Circulation and Climate. Academic Press, pp. 271-
745   302.

746   Roberts, J., Gottschalk, J., Skinner, L.C., Peck, V.L., Kender, S., Elderfield, H., Waelbroeck, C.,
747   Vázquez Riveiros, N., Hodell, D.A., 2016. Evolution of South Atlantic density and chemical
748   stratification across the last deglaciation. Proc. Natl. Acad. Sci. U.S.A. 113, 514-519.

749 Robinson, L.F., Adkins, J.F., Frank, N., Gagnon, A.C., Prouty, N.G., Roark, E.B., van de Flierdt, T.,
750 2014. The geochemistry of deep-sea coral skeletons: A review of vital effects and applications for
751 palaeoceanography. Deep Sea Research Part II: Topical Studies in Oceanography 99, 184-198.

752 Robinson, L.F., van de Flierdt, T., 2009. Southern Ocean evidence for reduced export of North
753 Atlantic Deep Water during Heinrich event 1. Geology 37, 195-198.

754 Shemesh, A., Hodell, D., Crosta, X., Kanfoush, S., Charles, C., Guilderson, T., 2002. Sequence of
755 events during the last deglaciation in Southern Ocean sediments and Antarctic ice cores.
756 Paleoceanography 17, 1056, doi: 1010.1029/2000PA000599.

757 Sigman, D.M., Hain, M.P., Haug, G.H., 2010. The polar ocean and glacial cycles in atmospheric CO_2
758 concentration. Nature 466, 47-55.

759 Sikes, E.L., Allen, K.A., Lund, D.C., 2017. Enhanced $\delta^{13}C$ and $\delta^{18}O$ differences between the South
760 Atlantic and South Pacific during the last glaciation: The deep gateway hypothesis. Paleoceanography
761 32, 1000-1017.

762 Skinner, L.C., 2009. Glacial-interglacial atmospheric CO_2 change: a possible "standing volume" effect
763 on deep-ocean carbon sequestration. Clim. Past. 5, 537-550.

764 Skinner, L.C., Fallon, S., Waelbroeck, C., Michel, E., Barker, S., 2010. Ventilation of the deep
765 Southern Ocean and deglacial CO_2 rise. Science 328, 1147-1151.

766 Skinner, L.C., Primeau, F., Freeman, E., de la Fuente, M., Goodwin, P.A., Gottschalk, J., Huang, E.,
767 McCave, I.N., Noble, T.L., Scrivner, A.E., 2017. Radiocarbon constraints on the glacial ocean
768 circulation and its impact on atmospheric CO2. Nature Communications 8, 16010, doi:
769 16010.11038/ncomms16010.

770 Skinner, L.C., Scrivner, A.E., Vance, D., Barker, S., Fallon, S., Waelbroeck, C., 2013. North Atlantic
771 versus Southern Ocean contributions to a deglacial surge in deep ocean ventilation. Geology 41, 667-
772 670.

773 Smith, J.A., Hillenbrand, C.-D., Pudsey, C.J., Allen, C.S., Graham, A.G.C., 2010. The presence of
774 polynyas in the Weddell Sea during the Last Glacial Period with implications for the reconstruction of
775 sea-ice limits and ice sheet history. Earth Planet. Sci. Lett. 296, 287-298.

776 Stein, K., Timmermann, A., Kwon, E.Y., Friedrich, T., 2020. Timing and magnitude of Southern
777 Ocean sea ice/carbon cycle feedbacks. Proc. Natl. Acad. Sci. U.S.A. 117, 4498-4504.

778 Struve, T., van de Flierdt, T., Burke, A., Robinson, L.F., Hammond, S.J., Crocket, K.C., Bradtmiller,
779 L.I., Auro, M.E., Mohamed, K.J., White, N.J., 2017. Neodymium isotopes and concentrations in
780 aragonitic scleractinian cold-water coral skeletons - Modern calibration and evaluation of palaeo-
781 applications. Chemical Geology 453, 146-168.

782 Struve, T., van de Flierdt, T., Robinson, L.F., Bradtmiller, L.I., Hines, S.K., Adkins, J.F., Lambelet,
783 M., Crocket, K.C., Kreissig, K., Coles, B., Auro, M.E., 2016. Neodymium isotope analyses after
784 combined extraction of actinide and lanthanide elements from seawater and deep-sea coral aragonite.
785 Geochemistry, Geophysics, Geosystems 17, 232-240.

786 Struve, T., Wilson, D.J., van de Flierdt, T., Pratt, N., Crocket, K.C., 2020. Middle Holocene
787 expansion of Pacific Deep Water into the Southern Ocean. Proc. Natl. Acad. Sci. U.S.A. 117, 889-
788 894.

789 Sudre, J., Garçon, V., Provost, C., Sennéchael, N., Huhn, O., Lacombe, M., 2011. Short-term
790 variations of deep water masses in Drake Passage revealed by a multiparametric analysis of the ANT-
791 XXIII/3 bottle data. Deep Sea Research Part II: Topical Studies in Oceanography 58, 2592-2612.

792 Talley, L.D., 2013. Closure of the global overturning circulation through the Indian, Pacific, and
793 Southern Oceans: Schematics and Transports. Oceanography 26, 80-97.

794 Toggweiler, J.R., 1999. Variation of atmospheric CO_2 by ventilation of the ocean's deepest water.
795 Paleoceanography 14, 571-588.

796 van de Flierdt, T., Griffiths, A.M., Lambelet, M., Little, S.H., Stichel, T., Wilson, D.J., 2016.
797 Neodymium in the oceans: a global database, a regional comparison and implications for
798 palaeoceanographic research. Philosophical Transactions of the Royal Society A: Mathematical,
799 Physical and Engineering Sciences 374, doi: 10.1098/rsta.2015.0293.

800 van de Flierdt, T., Robinson, L.F., Adkins, J.F., 2010. Deep-sea coral aragonite as a recorder for the
801 neodymium isotopic composition of seawater. Geochim. Cosmochim. Acta 74, 6014-6032.

802 WAIS Divide Project Members, 2013. Onset of deglacial warming in West Antarctica driven by local
803 orbital forcing. Nature 500, 440-444.

804 WAIS Divide Project Members, 2015. Precise interpolar phasing of abrupt climate change during the
805 last ice age. Nature 520, 661-665.

806 Watson, A.J., Ledwell, J.R., Messias, M.-J., King, B.A., Mackay, N., Meredith, M.P., Mills, B.,
807 Naveira Garabato, A.C., 2013. Rapid cross-density ocean mixing at mid-depths in the Drake Passage
808 measured by tracer release. Nature 501, 408-411.

809 Weber, M.E., Clark, P.U., Ricken, W., Mitrovica, J.X., Hostetler, S.W., Kuhn, G., 2011.
810 Interhemispheric Ice-Sheet Synchronicity During the Last Glacial Maximum. Science 334, 1265-
811 1269.

812 Wilson, D.J., Piotrowski, A.M., Galy, A., Banakar, V.K., 2015. Interhemispheric controls on deep
813 ocean circulation and carbon chemistry during the last two glacial cycles. Paleoceanography 30, 621-
814 641.

815 Xiao, W., Esper, O., Gersonde, R., 2016. Last Glacial-Holocene climate variability in the Atlantic
816 sector of the Southern Ocean. Quat. Sci. Rev. 135, 115-137.

817 Yu, J., Menviel, L., Jin, Z.D., Thornalley, D.J.R., Barker, S., Marino, G., Rohling, E.J., Cai, Y.,
818 Zhang, F., Wang, X., Dai, Y., Chen, P., Broecker, W.S., 2016. Sequestration of carbon in the deep
819 Atlantic during the last glaciation. Nat. Geosci. 9, 319-324.

820 Zhao, N., Oppo, D.W., Huang, K.-F., Howe, J.N., Blusztajn, J., Keigwin, L.D., 2019. Glacial–
821 interglacial Nd isotope variability of North Atlantic Deep Water modulated by North American ice
822 sheet. Nature Communications 10, 5773, doi: 5710.1038/s41467-41019-13707-z.